

Design and evaluation of a needle-to-ring electrohydrodynamic fan - experimental insights for airflow management

Klaudia Zwolińska-Gładys^{1*}, Jean Paul Cardona Murillo², Marek Borowski¹, Marek Różycki³ and Marek Jaszczur²

¹ AGH University of Krakow, Faculty of Civil Engineering and Resource Management, A. Mickiewicza 30, 30-059 Krakow, Poland

² AGH University of Krakow, Faculty of Energy and Fuels, A. Mickiewicza 30, 30-059 Kraków, Poland

³ m/d/t/k Trusted Advisers Group Sp. z o.o. ul. Rybnicka 43, 43-190 Mikołów, Poland

Abstract. The increasing demand for compact, energy-efficient, and quiet cooling and ventilation systems has prompted the exploration of alternatives to conventional mechanical fans. Conventional high-speed fans, however, often suffer from excessive noise and limited adaptability to modern miniaturized devices. In this work, an electrohydrodynamic (EHD) fan is introduced as a potential solution. The device employs a bladeless configuration with two electrodes, a high-voltage emitting needle and a grounded ring, to generate airflow through corona discharge and ionization. A configurable experimental prototype was constructed to evaluate different operational setups. Particle Image Velocimetry was applied to characterize the induced velocity fields. The experimental results demonstrated the generation of directional and controllable airflow patterns, confirming both the feasibility and effectiveness of the EHD approach. The study focused on analyzing the flow generated in the inter-electrode gap and the underlying mechanisms of corona discharge. The results allowed the identification of appropriate configurations and the optimal operating conditions for the prototype. These findings demonstrate that EHD fans hold significant potential for thermal management in electronics and advanced ventilation systems, where low noise and compactness are essential.

1 Introduction

The demand for compact and energy-efficient cooling and ventilation systems has increased in recent years with the miniaturization of electronic devices and stricter acoustic requirements. Conventional mechanical fans are widely used but often suffer from high noise levels and limitations in adapting to small form factors. These fans rely on moving parts that generate noise, experience wear, and become difficult to scale down for miniaturized applications. As a result, alternative airflow technologies that combine efficiency, reliability, and compactness are being pursued.

Electrohydrodynamic (EHD) fans or ionic jets have emerged as a promising bladeless solution. These devices utilize corona discharge, where ions are generated and accelerated within an electric field, to transfer momentum to neutral air molecules and induce airflow [1,2]. This mechanism eliminates moving components, offering the advantages of low noise, reduced mechanical complexity, and inherent scalability to miniaturized systems [3]. Indeed, EHD fans have no moving parts and thus operate with minimal acoustic noise, as well as their geometry makes them easy to miniaturize and even integrate directly into microelectronic packages. However, some studies suggest that EHD cooling devices can generate airflow with only a modest power input, aligning with the goal of energy-efficient design [1].

Previous research in the area of corona discharge-produced flows has primarily focused on macroscopic characteristics, such as outlet velocity, volumetric flow rate, or thermal dissipation efficiency [4]. Research on EHD fans specifically has examined different electrode pair geometries, such as needle-plate, wire-plate, or needle-ring, along with variations in applied voltage and the effects of grounded versus oppositely charged electrodes [5–7]. Studying them from both experimental and computational approaches. These works demonstrate the working principles, flexibility, and feasibility of this solution, while providing limited insight into the specific flow processes occurring directly between the electrodes [4].

The inter-electrode region involves critical phenomena such as ionization, charge acceleration, and momentum transfer events. An area of high electric field forms near the emitter tip, where electrons are stripped from electrically neutral air molecules. As a result, positive ions drift toward the grounded electrode, creating collisions with neutral air molecules. This ion-induced “wind” generates the bulk airflow between the electrodes. This region is sometimes considered as a sum of parts, the ionization region where ionization occurs, and the drift region where momentum is transferred by collisions due to the free electrons not having enough energy to ionize [8,9]. For a more complete understanding of EHD fan feasibility and as

* Corresponding author: kzwolinska@agh.edu.pl

a basis for future design optimization, it becomes important to resolve the dynamics in this core region.

The present work aims to address this gap by experimentally investigating flow formation and regimes in the inter-electrode region of a needle–ring EHD fan geometry. A configurable prototype was developed to allow variation of the electrode spacing and applied voltage, and Particle Image Velocimetry (PIV) was employed to directly capture velocity fields in the inter-electrode area. The results provide new insight into airflow development in this core region, including flow escape paths and the influence of electrode spacing and voltage on flow intensity and directionality. These findings advance the fundamental understanding of ion-driven flows and support future optimization of EHD fan design for efficient and low-noise ventilation and electronic cooling applications.

2 Methodology

For this research, the needle-cylinder geometry shown in Figures 1(a)–(b) was selected. This configuration was chosen due to its ease of construction, which allows for numerous potential extensions, as well as its axisymmetric nature, which is advantageous in many applications.

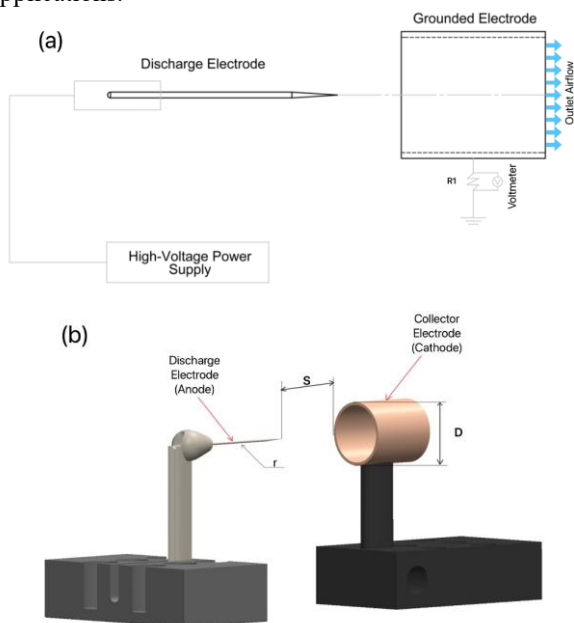


Fig. 1. Schematic of the needle-to-cylinder configuration: (a) electric wiring and (b) set-up view.

Two linear stages were used to mount the electrode holders; these allowed for horizontal adjustment and convenient cable management to facilitate needle centring and adjustment of the inter-electrode distance. The electrode installed along the cylinder axis was a steel needle with radius $r = 0.5$ mm and a copper cylinder of diameter $D = 22$ mm and wall thickness 1 mm. Three electrode spacings (S) were investigated: 0 mm, 11 mm, and 22 mm, corresponding to zero, half, and one-cylinder external diameter (D).

The holders were printed from black matte PLA using an FDM printer. After installing the electrodes, the assembly was mounted and fastened to Bakelite plates

to ensure electrical insulation. A Genvolt 74060P HV PSU, 0–40 kV, 1.5 mA, 60 W, +ve power supply with electric current and voltage measurements was applied. Additionally, in order to measure the electrical current from the cathode to the ground, a precision series resistor ($R1 = 99.1$ k Ω) was added in the ground line together with voltage measurements. The high-voltage (positive ground) output from the power supply was connected to the needle electrode and the copper tube was grounded.

Particle Image Velocimetry (PIV) and hot-wire anemometry were employed as measurement techniques to acquire detailed data on fluid flow.

To obtain detailed information about the flow characteristics in the inter-electrode region and the downstream, a planar PIV technique was employed. The experimental setup utilized a single-camera configuration with an Imager CX12 (LaVision, 12-bit) camera, offering a spatial resolution of 4080×2984 pixels. The measurement plane corresponded to a vertical cross-section of the cylindrical region, as illustrated in Figure 2.

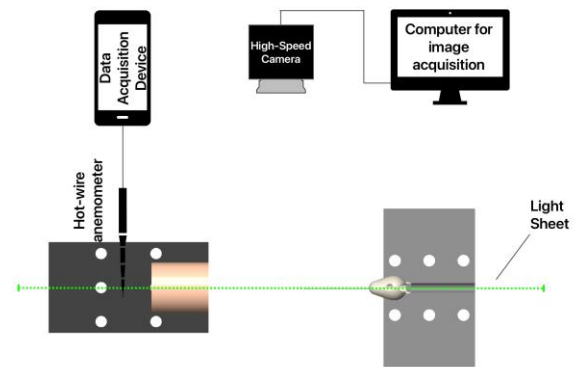


Fig. 2. Diagram of PIV setup showing illumination plane, electrodes, and camera orientation.

Velocity measurements were performed within this cross-section, encompassing both the inter-electrode area and the downstream region at the outlet of the tube-type electrode. The measurement plane was illuminated by a double-pulsed Nd:YAG laser (532 nm, 50 mJ per pulse). A thin laser sheet was formed using a combination of cylindrical and spherical lenses to ensure uniform illumination across the field of view. Di(2-ethylhexyl) sebacate (DEHS) droplets, with a mean diameter of approximately $1 \mu\text{m}$, were used as seeding particles to accurately trace the flow. Image acquisition was synchronized via a timing controller to coordinate the laser pulses with camera exposures. For each test condition, image pairs were recorded with individually optimized time steps to maximize particle displacement and enhance measurement accuracy. To ensure statistical reliability, 100 image pairs were acquired at each operating condition at a frame rate of 15 Hz.

The acquired images were processed using DaVis 11.2 software (LaVision GmbH). Velocity fields were computed using a multi-pass cross-correlation algorithm with progressively refined interrogation window sizes, decreasing from 64×64 to 32×32 pixels with a 75% overlap. The resulting instantaneous velocity vectors

were ensemble-averaged to obtain mean flow fields. These averaged velocity distributions were subsequently analysed to characterize airflow generation within the inter-electrode region, flow behaviour at the electrode outlet, and the influence of electrode spacing and applied voltage on flow dynamics.

A hot wire anemometer was used to measure the axial fluid flow velocity at the exit of the device to complement the PIV data. Using the connected Data acquisition device for the anemometer, measurements were taken during 60 seconds at 1-second intervals. Hot-wire measurement and current measurements were carried out starting from the lowest voltage at which a measurable current appeared and were continued at regular voltage intervals until breakdown occurred. For each electrode spacing, two voltages corresponding to low and high voltages were selected for detailed fluid flow measurements using Particle Image Velocimetry.

3 Results

3.1 Hot Wire Anemometry

Figures 3 and 4 present the results of outlet velocity measurements obtained using hot-wire anemometry. These figures illustrate the influence of the applied high voltage between the electrodes on the mean air velocity at the cylinder outlet. The results are shown for three different electrode spacings, $S = 0$ mm, 11 mm, and 22 mm. Time-averaged velocity values were measured at a distance of 11 mm from the outlet for the corresponding applied voltage, as summarized in Figure 3. In this Figure, a clear trend is observed: the outlet velocity increases consistently with the applied voltage for all electrode spacings. This behaviour agrees with observations reported in previous literature on electrohydrodynamic or corona-induced airflow phenomena.

It can also be seen that at shorter inter-electrode distances, lower voltages are required to achieve similar velocities compared with larger spacings. This is attributed to the stronger electric field intensity that develops between the electrodes at smaller separations, resulting in enhanced ion generation and momentum transfer to the surrounding air.

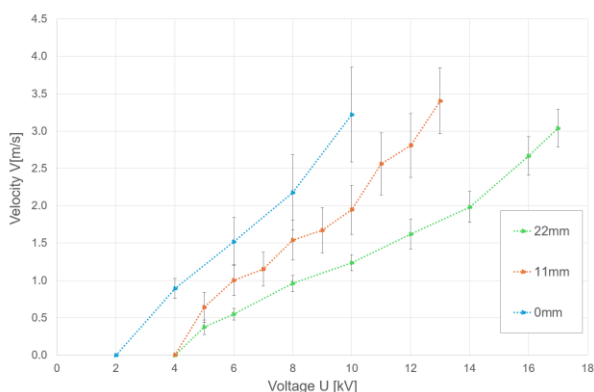


Fig. 3. Time-averaged air velocity at the outlet for three electrode spacings ($S = 0$ mm, 11 mm, and 22 mm) with corresponding velocity fluctuations shown as bars.

Furthermore, a clearly similar velocity is observed for the upper limit of the operational range for each configuration. As the applied high-voltage approaches limit, the system rapidly transitions to breakdown conditions, leading to an electrical discharge that terminates stable operation. This threshold behaviour was consistent across all tested geometries, indicating that the breakdown voltage is primarily governed by the electrode spacing and local field enhancement at the needle tip.

In Figure 4, velocity fluctuations are represented as bars, illustrating the unsteadiness of the generated flow. These fluctuations increase slightly with applied voltage, suggesting that higher ionization levels and stronger EHD interactions contribute to more turbulent flow structures near the outlet.

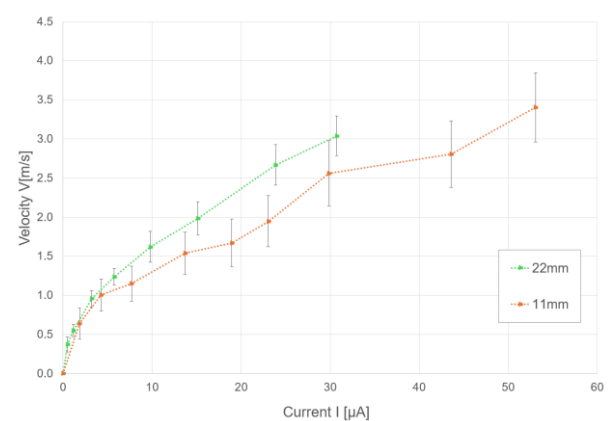


Fig. 4. Time-averaged air velocity at the outlet for two electrode spacings ($S = 11$ mm and 22 mm) with corresponding velocity fluctuations shown as bars.

In Figure 4, time-averaged air velocity at the cylinder outlet is presented for two different electrode spacings, $S = 11$ mm and 22 mm. Higher outlet velocities required correspondingly higher electrical currents, which in turn increased the electrical power necessary to sustain the generated flow. Velocity fluctuations are also shown as bars, indicating the degree of unsteadiness in the generated flow, which becomes more pronounced at higher operating electric current.

3.2 PIV

In the subsequent stage of the study, airflow patterns were analysed using the PIV measurement results to evaluate the control of flow direction and to assess the influence of electrode spacing on the velocity distribution at the outlet of the collector electrode. To obtain a more comprehensive understanding of the flow behaviour, three electrode distances were investigated. For each configuration, two voltage levels were selected for detailed analysis, representing the applicable operating range, corresponding to low- and high-voltage conditions. The ensemble-averaged velocity vector fields derived from the PIV analysis were superimposed onto the corresponding electrode geometry contours for all tested configurations. These composite visualizations

are presented as image pairs for each electrode distance, as described in the preceding section.

3.2.1 Electrode spacing: 0 mm

For the electrode spacing of 0 mm, corresponding to the configuration in which the electrodes are aligned, the applied low and high voltage values were 4 kV and 8 kV, respectively. The resulting flow fields are presented in Figures 5a and 5b. The figure also reveals the airflow patterns around the needle-type electrode, which occur as a consequence of the electrode alignment.

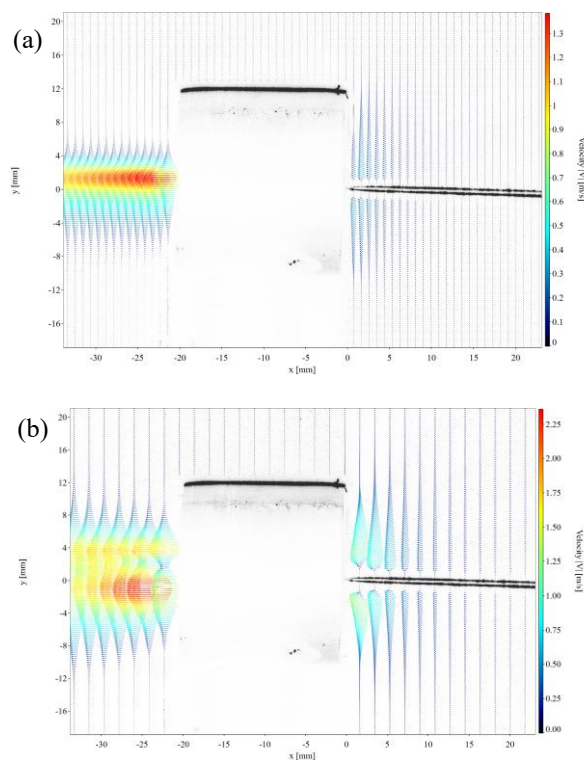


Fig. 5. Velocity fields at 0 mm for 4 kV (a) and 8 kV (b).

It is evident from both cases that a focused, unidirectional airflow is established at the outlet of the device, with a noticeable increase in velocity at higher applied voltages and a centrally concentrated distribution at the outlet of the collector electrode. Furthermore, in the inter-electrode region, a suction effect from the surrounding air is observed, indicating that the device accelerates not only particles aligned coaxially with the electrodes but also entrains ambient air to sustain the accelerated flow. Finally, it should be noted that in both operating conditions, the airflow around the external surfaces of the device is negligible. The flow remains highly concentric with respect to the electrodes, with the highest velocities occurring near the center of the collector electrode. In contrast, near the electrode wall, the velocity approaches zero, forming so-called “dead zones” in the outer regions of the ring-shaped collector electrode.

3.2.2 Electrode spacing: 11 mm

For the half-diameter electrode spacing, corresponding to 11 mm, the applied low and high voltage values were 6 kV and 14 kV, respectively. The corresponding velocity vector fields are presented in Figure 6.

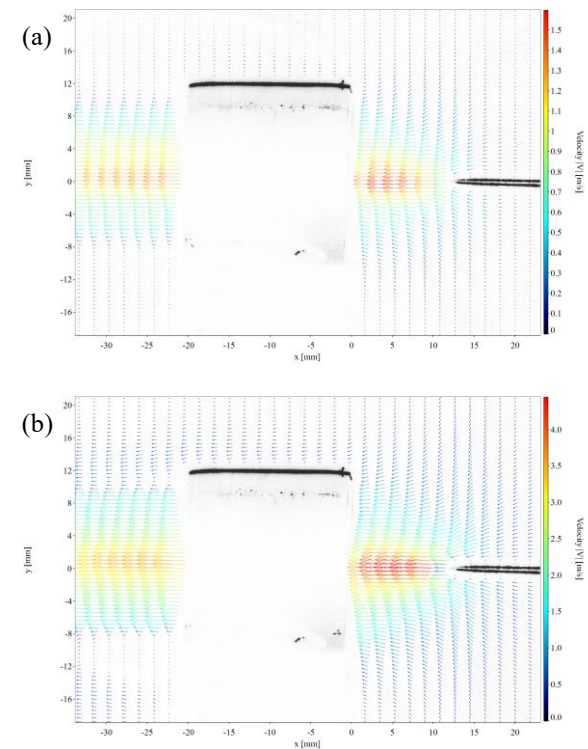


Fig. 6. Velocity fields at 11 mm for 6 kV (a) and 14 kV (b).

As observed for the previous electrode spacing, the trends of increasing airflow velocity with higher applied voltage and the formation of a focused jet are again evident. Similarly, within the inter-electrode region, suction and acceleration effects are clearly observed, with higher velocities concentrated near the needle electrode and along its axis. At higher voltage, a minor external airflow in the same direction as the outlet jet is also discernible outside the device. Unlike the previous configuration, in this case, the airflow extends across nearly the entire outlet surface of the collector electrode. Although the velocity decreases toward the electrode walls, the overall velocity distribution is considerably more uniform. Examination of the region between the electrodes reveals distinct flowlines connecting the tip of the needle-type electrode to the inner surface of the collector electrode. These flowlines delineate a region of increased air velocity, forming a funnel-shaped flow structure from discharge to collector electrode.

3.2.3 Electrode spacing: 22 mm

Similarly, for the largest electrode spacing of 22 mm, the applied low and high voltage values were 10 kV and 16 kV, respectively. The corresponding velocity vector fields are presented in Figure 7.

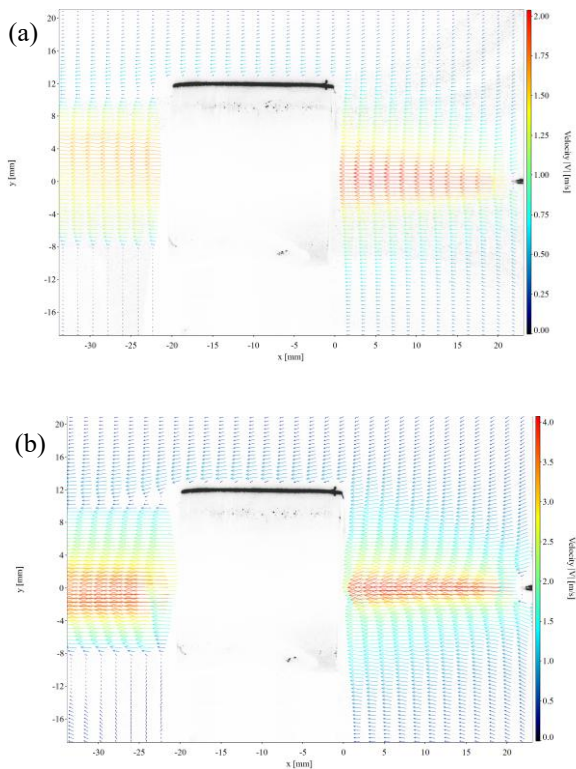


Fig. 7. Velocity fields at 22 mm for 10 kV (a) and 16 kV (b).

For the largest electrode spacing, the expected trend of increasing flow velocity with higher applied voltage is once again noticed. The flow pattern closely resembles that of the 11 mm configuration, with a distinct funnel-shaped structure that extends over a larger distance. The velocity distribution at the outlet of the collector electrode is more uniform, with higher velocities maintained along the central axis and decreasing toward the electrode walls. This uniformity is particularly noticeable at lower voltage levels (Fig. 7(a)). As the applied voltage increases, the flow becomes more axially oriented. Additionally, an external flow outside the device becomes more pronounced, especially under high-voltage conditions. Nonetheless, the overall character of the flow remained steady and axisymmetric for all tested configurations, confirming the stability of the setup within the pre-breakdown voltage range.

4 Conclusions

The presented results allow for an improved understanding of flow formation in the inter-electrode region. Contrary to expectations, the particle image velocity results show no flows outside of the cylinder at $S = 0$ mm electrode spacing, where radial ion flow was anticipated. Instead, in all configurations, radial suction occurs within the inter-electrode region. The highest velocity was achieved in the vicinity of the needle and along its axis. Even at larger electrode spacings and higher voltages, no evidence was found for significant flow escaping from the main direction. In selected cases, only a very weak external flow was observed. This flow appears to result from the formation of local negative pressure and the external disturbances, such as the minor effect of the seeding atomiser, rather than being generated directly by the ionic flow.

From PIV measurements with 11 mm and 22 mm electrode spacings, the flow profile at the collector electrode's inlet was nearly identical to that at its outlet, both in velocity magnitude and direction. This strongly indicates that most flow acceleration occurs in the inter-electrode region, and the collector electrode only minimally modifies or focuses the flow at smaller spacings. These observations suggest that the length of the collector electrode is not a significant factor in the resulting flow velocity.

Both Particle Image Velocimetry and hot-wire anemometry measurements showed the strong relationships between voltage, current, and velocity. There was a clear trend of increasing flow velocity with higher voltage, likely because higher voltage enhances electrohydrodynamic effects and promotes stronger jet formation or ion-driven acceleration. Additionally, the flow becomes more uniform at the outlet when the spacing between electrodes is increased, likely because a larger distance allows for better flow development. However, at larger electrode spacings, higher voltage and current were required to achieve velocities that could be obtained at lower voltages and currents with smaller spacings.

Ultimately, these conclusions underline the potential of this approach for airflow generation. There are clear effects of applied voltage on flow velocity and electrode spacing on flow uniformity. The approach is effective across a wide range of operating conditions and configurations that could be applied to real-world problems, with the main drawback being that larger spacings require higher voltages and electrical currents to achieve comparable flow speeds. Most importantly, the radial suction effect observed in the inter-electrode region and the subsequent axially focused flow demonstrate the device's effectiveness in generating directed flow. The absence of radial flow components at the outlet is a promising result, as such flows would have led to energy losses in the system.

Based on these findings, future research could aim to verify the repeatability of these results with smaller ring-shaped collector electrodes to assess whether collector length influences the resulting flow characteristics. Moreover, investigating the effects of air properties, such as humidity, temperature, or different seeding particles, on the velocity field could contribute to a more comprehensive understanding of the flow behaviour. The literature contains studies confirming the possibility of using the PIV technique in experiments with a strong electric field. Nevertheless, the authors highlight the potential influence of seeding on the electrohydrodynamic effect, particularly regarding modifications of the electrical properties of the air and the distortion of the electric field distribution caused by the presence of tracer particles. This matter will be the subject of further research. Finally, coupling these experimental results with numerical simulations and developing different geometries or configurations could offer deeper insights into the operation and performance range of such devices. Collectively, these efforts would support the future development of these devices for use as quiet, static flow generators for practical applications.

Fundings: This work was partly funded by AGH University of Krakow, Faculty of Civil Engineering and Resource Management (No. 501.00-100302-10000) and Faculty of Energy and Fuels (No. 500.00-210000-10000).

Data availability statement: Data will be made available on request

References

1. Y. Peng, D. Li, X. Yang, Z. Ma, Z. Mao, A Review on Electrohydrodynamic (EHD) Pump, *Micromachines*. **14**, 321 (2023). <https://doi.org/10.3390/mi14020321>
2. J. Wang, R. Cai, T. Zhu, Y. Liu, Ionic Wind Intensity Enhancement and Ozone Reduction in a Solid-State Fan Via Electromagnetic Field Action, *Plasma Chemistry and Plasma Processing*. **42**, 1045–1067 (2022). <https://doi.org/10.1007/s11090-022-10273-z>
3. S.-F. Cheng, J.C. Leong, F.C. Lai, EHD gas pump as a cooling device for electronic components in a horizontal channel. *Journal of Electrostatics*. <https://doi.org/10.1016/j.elstat.2024.103935>
4. J. Wang, Z. Tao, Y. X. Cai, J.-B. Wang, J. Wang, Development and application of a solid-state fan for enhanced heat dissipation. *Appl. Therm. Eng.* **169**, 114922 (2020). <https://doi.org/10.1016/j.applthermaleng.2020.114922>
5. Y. Birhane, S. C. Lin and F. C. Lai, Flow characteristics of a two stage EHD gas pump in circular pipe. 2015 IEEE Industry Applications Society Annual Meeting, Addison, TX, USA. 1-9, (2015). <https://doi.org/10.1109/IAS.2015.7356769>
6. B. Halim, A. Dehghanhadikolaei, O. Amili, H. Sojoudi, Understanding electrohydrodynamic (EHD) performance of corona discharge via particle image velocimetry (PIV). *SN Appl. Sci.* **5**, 33 (2023). <https://doi.org/10.1007/s42452-022-05217-3>
7. A. Ramadhan, N. Kapur, J. Summers, H. Thompson, Numerical Development of EHD Cooling Systems for Laptop Applications. *Applied Thermal Engineering*. **139**, 144–156 (2018). <https://doi.org/10.1016/j.applthermaleng.2018.04.119>
8. J. Mi, D. Xu, Y. Sun, S. Du, Y. Chen, Influence of magnetic fields on negative corona discharge currents. *J. Electrostat.* **66**, 457–462 (2008). <https://doi.org/10.1016/j.elstat.2008.04.010>
9. S. I. Wais, P. A. Mohammed, Influence of magnetic field on characteristics of corona discharge in wire-cylinder electrodes configuration. *Plasma*. **4**, 764-779 (2021). <https://doi.org/10.3390/plasma4040039>